

Posted: 14.03.2023

Geometric Basics and Calculation Methods for the Design of a Technical Saddle Joint based on Owl Neck Vertebrae

Johannes Gründer^{a,*}, Rüdiger Hornfeck^a

^a Nuremberg Institute of Technology, Kesslerplatz 12, 90489 Nuremberg, Germany

* Corresponding author. Tel.: +49-911-5880-1905; E-mail address: johannes.gruender@th-nuernberg.de

Abstract

A saddle joint enables the movement of two components relative to each other primarily about two axes of rotation and, to a limited extent, in translational direction. This type of joint is primarily found in nature, for example in the human thumb, in the ossicles and the cervical spine of owls. Motivated by the high degree of the owls' head mobility, the authors aim to make this high motion potential technically accessible by defining relevant design parameters and developing calculation methods for dimensioning the saddle joint components. First, an abstracted contact geometry model based on the owls' saddle joints is defined. A method for calculating the kinematics of the joint as a function of the previously introduced design parameters of the contact is derived mathematically. Regarding the implementation in a design process, this model is used to calculate the restoring forces required to stabilize the joint parts as well as the actuator torque needed for a specific rotational movement around those axes. Furthermore, the rotational stiffness of a specific joint geometry is calculated as an important design criterion. In summary, the defined contact geometry, the kinematics, and the computable forces serve as basis for designing technical saddle joints in the future.

Keywords: Bionics, Geometry, Kinematic, Mechanism, Saddle Joint, Simulation.

1. Learning from the Mobility of the Owl

A saddle joint enables the movement of two parts relative to each other primarily about two axes of rotation and, to a limited extent, in translational direction. This type of joint is primarily found in nature, for example in the human thumb, in the ossicles and the cervical spine of owls. The spine structure, the arrangement and attachment of muscles as well as the contact geometry of the vertebrae and the movement ability is well documented by Krings et al. [1, 2] and Boumans et al. [3].

At the Nuremberg Institute of Technology, Hornfeck and Löffler developed a prototype of a robotic arm according to the example of the cervical spine of owls in [4] to adapt the high degree of movement for the design in a robot arm. In contrast to the biological example, the rotational movement was not

implemented by 14 saddle joints with two axes, but by 28 rotary joints with one rotational axis each. The feasibility as well as the high mobility of a robot arm with these specific joints could be proven within the scope of the project. Shape memory alloy wires were used as actuators while the joint components were additively manufactured.

To further develop this principle of high mobility for robot arms, the authors aim to develop a technically usable saddle joint to reduce the complexity and number of joints needed for this type of design. For this purpose, basic geometric parameters of a technical saddle joint are defined and described in the following and a calculation method for the design of saddle joints is developed.

Nomenclature

a	Side length of the force plane
c_R	Rotational stiffness
d	Distance between initial contact point and force plane
k	Spring stiffness
\vec{n}_K	Working direction of the resulting forces
\vec{n}_{KU}	Normal vectors of the lower contact surface
\vec{n}_U	Generating axis
\vec{n}_{x-x}	Rotational axis of the saddle joint in x-direction
\vec{n}_{y-y}	Rotational axis of the saddle joint in y-direction
u	Displacement
r_1	Radius of the convex circle
r_2	Radius of the concave circle
x, y, z	Cartesian coordinate directions
F	Spring force
F_K	Contact forces
F_V	Spring preload force
F_u	Spring force due to point displacement
K	Contact point
K_0	Contact point in initial saddle joint position
K_O	Upper contact surface
K_U	Lower contact surface
L_0	Initial spring length
L	Spring length
M	Torque
P_O	Spring fixation points of the upper saddle joint part
P_U	Spring fixation points on the lower saddle joint part
R	Rotational matrix
\vec{U}	Origin of coordinates
α	Opening angle of the contact surfaces
β	Generating angle of the contact surfaces
γ	Generating angle of the contact surfaces
δ	Clearance of the saddle joint
φ	Rotational angle of the saddle joint

2. Geometry and Kinematics of the Technical Saddle Joint

2.1. Owl vertebrae geometry and contact surfaces

According to Krings et al. [1], each of the 14 different cervical vertebrae of the owl allows specific rotation angles. The contacts between two vertebrae consist of a concave and a convex surface like a saddle joint, whereby in nature there is always an intervertebral disc between the components to prevent bone to bone contact. The saddle joint consists of a rider and a saddle as one joint part sits like a rider in the saddle of the adjacent joint part. The joint consisting of very similar contact surfaces is aimed to be made technically usable in this paper by a suitable description and definition, whereby the operating behaviour of the saddle joint can be pre-determined by the presented equations during the design phase.

Figure 1 shows the model of the technical adaptation, where only the lower half of a saddle joint in initial position is displayed. In the model, the lower part consists of the contact surface $K_U = f(r_1, r_2, \alpha, \beta, \gamma)$ (see Figure 2) acting as the saddle and the square plane F_U with edge length a and distance d to the contact point \vec{K}_0 in the initial position with the contact surface K_O acting as the rider. Under any angular position other than the initial, the contact point \vec{K}_0 moves from its initial position and is called \vec{K} . This point is always located on both contact surfaces. In the plane F_U , the fixation points of the four restoring elements (in nature: muscles) between the lower and upper joint parts are in $\vec{P}_{U,1}$ to $\vec{P}_{U,4}$. The muscle behaviour is linearised and modelled like mechanical springs. The coordinate origin $\vec{U} = (0 | 0 | 0)$ with the coordinate axes x, y and z is defined in the location of the initial contact point \vec{K}_0 . The geometric shape of the contact area K_U is limited by the angle α to allow movement relative to the other joint part, depending on the choice of the other design parameters.

2.2. Contact surface Geometry

The contact surfaces of the rider and saddle are assumed geometrically identical, but may also be designed differently.

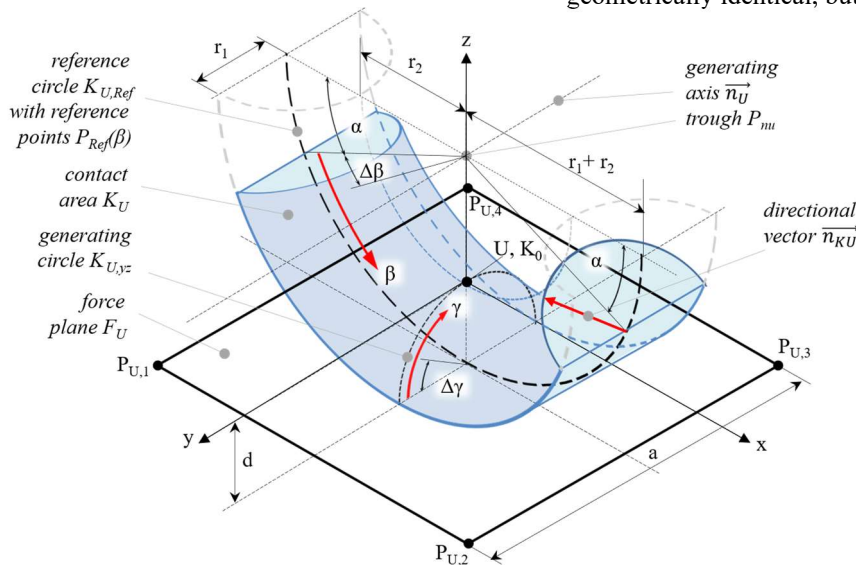


Fig. 1. Geometric parameters of the saddle joint model

The surfaces both consist of a concave and a convex region while the concave region defines the position of the respective axis of rotation $\vec{n}_U = \vec{n}_{y-y}$ or $\vec{n}_O = \vec{n}_{x-x}$ of each part of the saddle joint according to Figure 2.

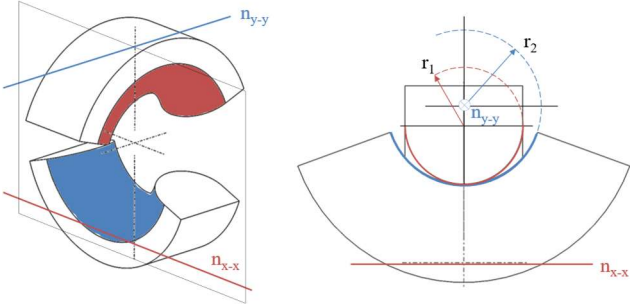


Fig. 2. Contact geometry of the saddle joint

The contact surfaces \mathbf{K}_U and \mathbf{K}_O are geometrically defined by the radius r_1 of the convex curvature and by the radius r_2 of the concave curvature in the section shown in Figure 2. The radii of the other component are located in the section plane, which is rotated by 90° . The radii of curvature of the contact surfaces are different in both x- and y-directions.

The contact surface \mathbf{K}_U (analogously also \mathbf{K}_O) is created by rotation of the generating semicircle $\mathbf{K}_{U,yz}$ located in the yz-plane with radius r_1 around the axis $\vec{n}_U = [0 \ 1 \ 0]$ through the point $\vec{P}_{nU} = (0 \ | \ 0 \ | \ r_2)$ with the angle $-\pi/2 + \alpha \leq \beta \leq \pi/2 + \alpha$ and the step size $\Delta\beta$. The semicircle $\mathbf{K}_{U,yz}$ is thereby calculated between $-\pi/2 \leq \gamma \leq \pi/2$ with step size $\Delta\gamma$. Before rotation around \vec{n}_U , $\mathbf{K}_{U,yz}$ is shifted by $|\vec{U} \vec{P}_{nU}|$ from the origin and transformed back by the same amount after rotation. The contact surface \mathbf{K}_U is calculated according to equation (1):

$$\mathbf{K}_U = \left[\begin{pmatrix} 0 \\ \sin(\gamma) \cdot r_1 \\ \cos(\gamma) \cdot r_1 - r_2 \end{pmatrix} - |\vec{U} \vec{P}_{nU}| \right] \cdot R(\beta, n_u) + |\vec{U} \vec{P}_{nU}| \quad (1)$$

For calculating the spring forces and the contact force, the normal vectors on each contact surface are calculated. The contact point \vec{K}_O is moving on the contact surfaces \mathbf{K}_U and \mathbf{K}_O depending on the direction of the spring forces. For the calculation of the normal vectors, the reference circle $\mathbf{K}_{U,Ref}$ located in the xz-plane around the axis \vec{n}_U with $r = r_1 + r_2$ is introduced. The circle is calculated for the same angles β as the points on the contact surface \mathbf{K}_U and in the same step size. Thus, for all points located on a semicircle $\mathbf{K}_{U,yz}(\beta)$ rotated with angle β around the axis \vec{n}_U and originating from $\mathbf{K}_{U,yz}$, a point $\vec{P}_{Ref}(\beta)$ is created as direction reference to these points with distance $|\vec{P}_{Ref} \vec{K}_U| = r_1$. The directional vector \vec{n}_{KU} of each point of the contact surface \mathbf{K}_U is calculated according to equation (2):

$$\vec{n}_{KU} = \frac{\begin{pmatrix} \sin(\beta) \cdot (r_1 + r_2) \\ 0 \\ -\cos(\beta) \cdot (r_1 + r_2) + r_2 \end{pmatrix} - \mathbf{K}_U(\beta, \gamma)}{r_1} \quad (2)$$

2.3. Kinematics

As shown in Figure 2, the axis of rotation \vec{n}_O of surface \mathbf{K}_O and \vec{n}_U of surface \mathbf{K}_U are each located in the respective other joint part. In a saddle joint, these axes are always at an angle to each other and can never intersect. In the model, the kinematics are considered for a single saddle joint, detached from a larger context such as a robot arm. Therefore, a pure motion of the upper joint part around both axes is described, while the lower joint part is fixed. A rotation around the axis \vec{n}_{y-y} thus results in a change of position and orientation of \vec{n}_{x-x} . A rotation around \vec{n}_{x-x} , on the other hand, leaves the position and orientation of the axis \vec{n}_{y-y} unchanged. The rotational angles of the upper part of the joint are φ_{x-x} and/or φ_{y-y} . Figure 3 shows the upper joint part in the individual rotation directions.

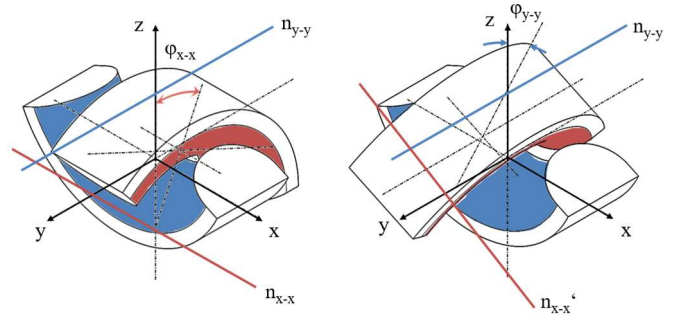


Fig. 3. Kinematics of the saddle joint

The rotation of the upper joint part is calculated using the general rotational matrices \mathbf{R}_{x-x} and \mathbf{R}_{y-y} for the specific rotational angle as given by [5] in equation (3) and (4):

$$\mathbf{R}_{x-x} = \begin{pmatrix} 1 & 0 & 0 \\ 0 & \cos(\varphi_{x-x}) & -\sin(\varphi_{x-x}) \\ 0 & \sin(\varphi_{x-x}) & \cos(\varphi_{x-x}) \end{pmatrix} \quad (3)$$

$$\mathbf{R}_{y-y} = \begin{pmatrix} \cos(\varphi_{y-y}) & 0 & \sin(\varphi_{y-y}) \\ 0 & 1 & 0 \\ -\sin(\varphi_{y-y}) & 0 & \cos(\varphi_{y-y}) \end{pmatrix} \quad (4)$$

2.4. Translational and rotational clearance

Assuming the condition $r_1 < r_2$ and that there is always contact between the surfaces \mathbf{K}_O and \mathbf{K}_U , there is translational clearance in the x, y and z direction as well as a rotational clearance around the z axis. The amount of displacement of the upper relative to the lower joint part under load depends on the forces and their directions acting on the saddle joint. The maximum translational clearance occurring in a technical saddle joint can be determined directly from the design of the contact geometries. The largest possible displacement of the circle r_1 in the circle r_2 results for an angle $\alpha = 0^\circ$ or $\beta = 180^\circ$. Figure 4 shows the ratios for the calculation in the xz-plane of the maximum clearance for the case $\alpha > 0^\circ$. The calculation of the clearance δ_x and δ_z is derived in the xz-plane, the clearance

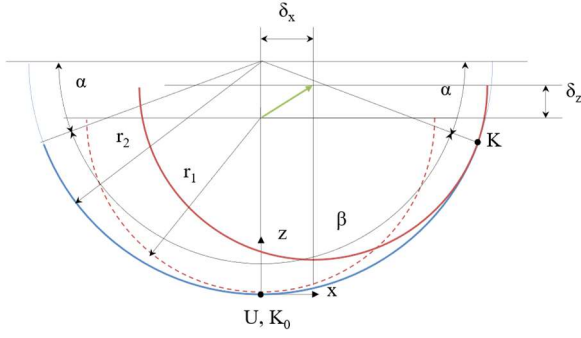


Fig. 4. Displacement of circle r_1 in circle r_2 in the xz -plane

δ_y in the yz -plane is calculated analogously to δ_x . The relative clearance of the joint assembly is calculated with respect to the larger radius r_2 according to equations (5) and (6).

$$\delta_x = \delta_y = \frac{\sin\left(\frac{\pi}{2} - \alpha\right) \cdot (r_2 - r_1)}{r_2} \quad (5)$$

$$\delta_z = \frac{\left(1 - \cos\left(\frac{\pi}{2} - \alpha\right)\right) \cdot (r_2 - r_1)}{r_2} \quad (6)$$

Solving these equations, the clearance of the saddle joint can be predetermined during the design phase. Figure 5 shows the relative clearance related to the larger radius r_2 as a function of the angle α .

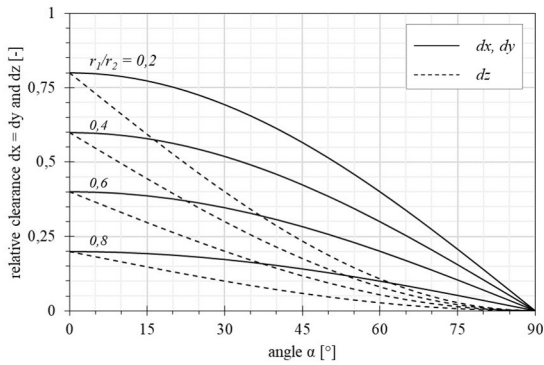


Fig. 5. Clearance δ in x , y and z depending on α

The rotational movement of the saddle joint around the z axis must be as small as possible to prevent unwanted torsion in operation although a minimum of clearance is needed to ensure the operation of the joint which can be solved by appropriate design of the joint periphery. With increasing translational clearance in z direction, the rotational clearance also increases. The rotational clearance is defined as the largest possible angle $\phi_{z-z,max}$ by which the upper contact surface K_0 can be rotated around the z axis until the upper and the lower contact surfaces are in contact. Figure 6 shows the relation between the geometric radii r_1 and r_2 and the translational displacement δ_z and the maximum rotation angle $\phi_{z-z,max}$.

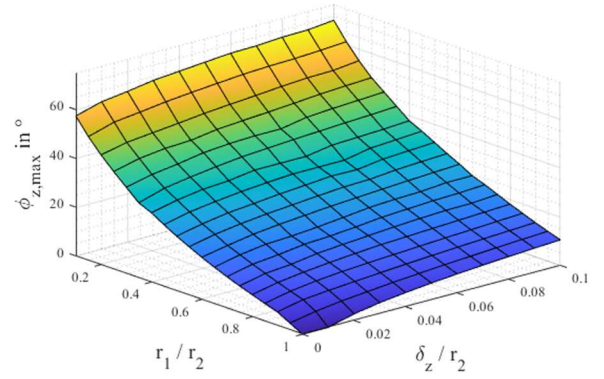


Fig. 6. Maximum free rotation angle $\phi_{z-z,max}$ around z -axis

3. Calculation Model

The spring forces acting on the saddle joint are calculated based on the considerations presented in chapter two. The model of the joint is additionally extended to include restoring elements, which provide stabilization on the one hand and to restore the joint to its initial position on the other. In contrast to the owl's cervical vertebrae, where a complex interaction of muscles and tendons is responsible for the movement of the joints, springs with a linear characteristic curve and the spring constant k are used for calculation. However, any force-elongation curves can be modelled to simulate the forces on an owl's neck vertebra. Four springs are used in the model, with each spring attached to a corner of the surfaces F_U and F_O . The arrangement is shown in Figure 7:

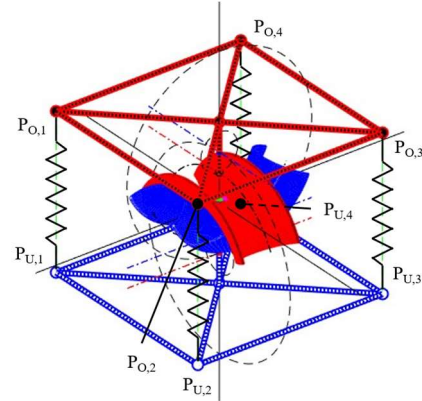


Fig. 7. Geometry of the model for calculating the forces (MATLAB)

To move the joint, an (at this point) undefined actuator system must now apply forces that are

- larger than the forces of the spring elements and
- counteracting the spring forces to hold an angular position.

Therefore, it is necessary to calculate the expected spring forces for a saddle joints design parameter configuration in advance for the design of the actuator system.

3.1. Force calculation

To calculate the spring forces, the upper joint part is rotated into every possible position. In the following, the calculation is derived for the forces \vec{F}_i of a spring between the points $\vec{P}_{U,i}$ and $\vec{P}_{O,i}$ with the spring constant k , the unstressed length \vec{L}_0 and the distance \vec{L}_i between the fix points in the initial position. The magnitude ratios for the displacement of the point $\vec{P}_{O,i}$ due to the rotation of the upper joint part into the point $\vec{P}_{O,i}'$ are shown in Figure 8:

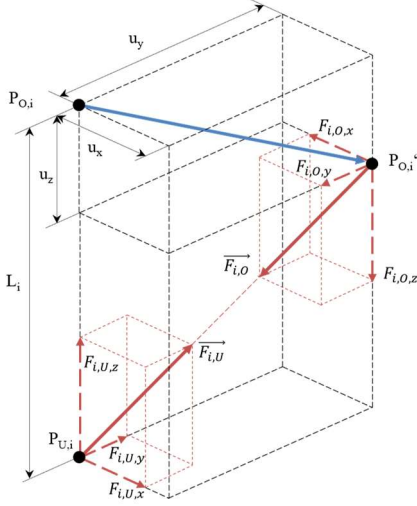


Fig. 8. Spring forces due to fix point displacement

The occurring spring forces $\vec{F}_{i,U}$ in any position of the upper joint part result from the overlaid preload force $\vec{F}_{i,V}$ and the strain- or compression-dependent force $\vec{F}_{i,u}$ according to equation (7):

$$\vec{F}_{i,U} = \vec{F}_{i,V} + \vec{F}_{i,u} \quad (7)$$

If the springs are preloaded, the installation length L_i between the rest positions of the fixed points $\vec{P}_{U,i}$ and $\vec{P}_{O,i}$ of the spring F_i in the zero position is unequal to the zero length L_0 . The preload force is calculated according to equation (8), where a positive preload force is defined as a compressive force and a negative one as a tensile force in the respective direction:

$$F_V = k \cdot (L_0 - L_i) = k \cdot (L_0 - |\overrightarrow{P_{U,i}P_{O,i}}|) \quad (8)$$

The spring forces F_u occurring in an angular position of the joint are added to the preload force F_V . They are calculated according to equation (9) by the respective distance between the points $\vec{P}_{U,i}$ and $\vec{P}_{O,i}$ at which the springs are fixed:

$$F_{i,u} = k \cdot u_i = k \cdot |\overrightarrow{P'_{O,i}P'_{U,i}}| \quad (9)$$

The load acting at the contact point \vec{K} is equal to the sum of the spring forces as it is acting as the bearing point when peripheral geometries and actuator forces are neglected. The contact force \vec{F}_K is calculated according to equation (10):

$$\vec{F}_K = \sum_{i=1}^n \vec{F}_i \quad (10)$$

The effective direction \vec{n}_K of \vec{F}_K is obtained by normalizing the force components in x, y and z to the total contact force according to equation (11):

$$\vec{n}_K = \frac{\vec{F}_K}{|\vec{F}_K|} \quad (11)$$

3.2. Rotation of the upper saddle joint part

To calculate the rotation of the upper joint part, the positions of the spring force application points $\vec{P}_{O,i}$ as well as the upper contact surface \mathbf{K}_O are rotated around the origin with the rotation matrix \mathbf{R} according to equation (3) and (4). The calculation is performed in equation (12) as an example for the rotation of the surface \mathbf{K}_O by the angle φ_{x-x} around the axis \vec{n}_{x-x} :

$$\mathbf{K}'_O = (\mathbf{K}_O - |\overrightarrow{U n_{x-x}}|) \cdot \mathbf{R}(\varphi_{x-x}, n_{x-x}) + |\overrightarrow{U n_{x-x}}| \quad (12)$$

3.3. Calculation of the contact point

The movement of the joint as well as the changing direction of the acting forces shift the contact point \vec{K} between the surfaces \mathbf{K}_U and \mathbf{K}_O depending on the angular position of the saddle joint. In a frictionless joint, as according to [6], the contact position of the convex body running in the concave is located at the point where both surface normal vectors point in the direction of the resulting forces. Since a change in the position of the upper joint part results in a change of the spring forces due to the new relative positions, the contact point \vec{K} is determined iteratively according to the calculation scheme in Figure 9:

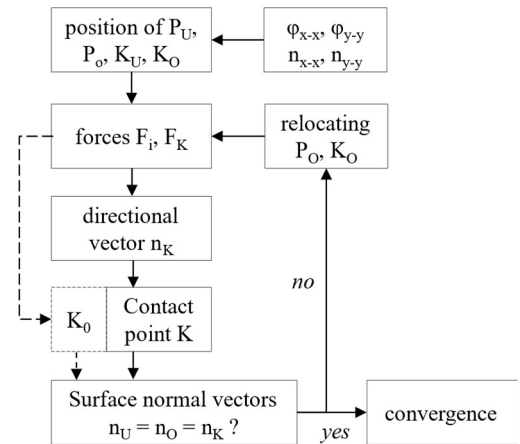


Fig. 9. Method for calculating the contact point

3.4. Rotational stiffness

The rotational stiffnesses $c_{R,x-x}$ and $c_{R,y-y}$ are defined as comparative quantities of different joint geometries. They both are functions of the angles φ_{x-x} and φ_{y-y} . The stiffness describes the torque M_A that must be applied by any actuator about the rotational axes to satisfy static equilibrium in any given angular position of the joint. The moment equilibria around the rotational axes of the joint are calculated according to equation (13):

$$\begin{aligned} \vec{M} &= \begin{pmatrix} M_{x-x} \\ M_{y-y} \end{pmatrix} \\ &= \begin{pmatrix} \Sigma(F_{U,i,y} \cdot d_{U,i,z}) + \Sigma(F_{U,i,z} \cdot d_{U,i,y}) \\ \Sigma(F_{U,i,x} \cdot d_{U,i,z}) + \Sigma(F_{U,i,z} \cdot d_{U,i,x}) \end{pmatrix} \end{aligned} \quad (13)$$

The stiffness about an axis \vec{n}_{j-j} is calculated according to equation (14):

$$c_{R,j-j}(\varphi_{j-j}) = \frac{M_{j-j}}{\varphi_{j-j}} \quad (14)$$

4. Calculation results

To calculate the stiffness of a specific parameter set, the position angles φ_{x-x} and φ_{y-y} are varied in the range covered by the joint and the torques around the corresponding axes are evaluated. The data used for the exemplary calculation is summarized in Table 1:

Table 1. Parameter values of the investigated saddle joint geometry.

Parameter	Unit	Value	Parameter	Unit	Value
r_1	[mm]	15	r_2	[mm]	25
d	[mm]	$40 - r_1$	L_0	[mm]	75
k	[N/mm]	10	a	[mm]	100
α	[°]	45	$\varphi_{x-x}, \varphi_{y-y}$	[°]	-15...15

Solving the proposed equations for this parameter set in a MATLAB simulation environment yields the stiffness $c_{R,x-x}$ as shown in Figure 10:

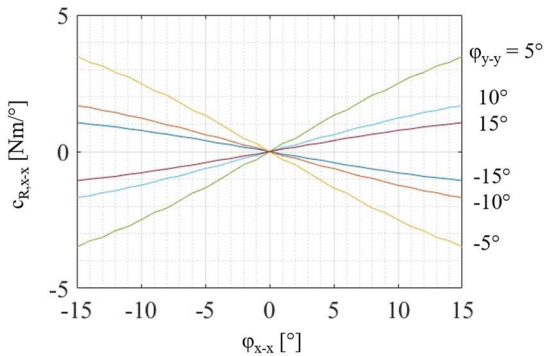


Fig. 10: Stiffness $c_{R,x-x}$ for the specific parameter set.

The contact point \vec{K} moves over the contact surfaces. Figure 11 shows the position of \vec{K} on the lower contact surface \mathbf{K}_U for the simulations projected in the xy -plane:

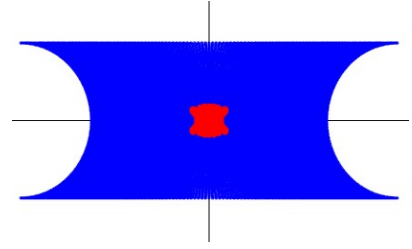


Fig. 11. Contacting area of the saddle joint geometry.

5. Conclusion

The defined geometric parameters and the calculation method for determining the restoring forces offer the possibility of dimensioning and designing saddle joints as an element of a robot arm. By suitable selection of the contact surface parameters, the joint clearance can be determined for translationally non-fixed parts and the expected loads on the joint can be calculated. This further enables the selection and pre-dimensioning of an actuator system for moving the joint. The detailed technical implementation of the saddle joint is up to the designer.

In addition, a more detailed load analysis of the saddle joint must be carried out. If a design is available, the expected material stress can be determined using the finite element method. Practical validation in the form of tests on a prototype can be the subject of future investigations.

Acknowledgements

The authors would like to thank the STAEDTLER Foundation for funding this research project.

References

- [1] Krings, M., Nyakatura J.A., Boumans, M., Fischer, M., Wagner, H. Barn owls maximize head rotations by a combination of yawing and rolling in functionally diverse regions of the neck. In: Journal of anatomy 231 (1), 2017, p. 12-22.
- [2] Krings, M., Nyakatura, J., Fischer, S., Wagner, H. The Cervical Spine of the American Barn Owl (*Tyto furcata pratincola*): I. Anatomy of the Vertebrae and Regionalisation in Their S-Shaped Arrangement. In: PloS one 9 (3), 2014.
- [3] Boumans, M., Krings, M., Wagner, H. Muscular Arrangement Sites in the Cervical Region of the American Barn Owl (*Tyto furcata pratincola*). In: PloS one 10 (7), 2015.
- [4] Hornfeck, R., Löffler, R., An owl neck joint for more efficient machines (de: Ein Eulenhalsgelenk für effizientere Maschinen), final report. Project funded by the Bavarian State Ministry for the Environment and Consumer Protection, 2022.
- [5] Goldhorn, K.H., Heinz, H.P., Kraus, M., Modern mathematical methods of physics volume 2 (de: Moderne mathematische Methoden der Physik Band 2), Springer-Verlag Berlin Heidelberg, 2010.
- [6] Nägerl, H., Kubein-Meesenburg, D., Cotta, H., Fanghänel, J., Kirsch, S. Biomechanical principles in diarthroses and synarthroses (de: Biomechanische Prinzipien in Diarthrosen und Synarthrosen), In: Z. Orthop. 131 (1993), p. 293-301.